inorganics

MDPI

Article

Structure–Function Relationship within Cu-Peptoid Electrocatalysts for Water Oxidation

Guilin Ruan, Natalia Fridman and Galia Maayan *

Schulich Faculty of Chemistry, Technion-Israel Institute of Technology Technion City, Haifa 3200008, Israel
* Correspondence: gm92@technion.ac.il

Abstract: Water oxidation (WO) is the first step in the water-splitting process aiming at the production of hydrogen as a green renewable fuel. To successfully perform WO, potent strategies for overcoming the high energetic barrier and slow kinetics of this reaction are urgently required. One such strategy is the use of molecular catalysis. Specifically, Cu-based catalysts have been highlighted over the last decade due to their stability and fast kinetics. Among them, Cu-peptoids, where peptoids are peptidomimetics akin to peptides and are N-substituted glycine oligomers, can act as stable and active catalysts for oxidation transformations including electrocatalytic WO. Previously, we suggested that a benzyl group incorporated as a side chain near the catalytic site within a Cu-peptoid electrocatalyst for WO has a structural role in the activity of the electrocatalyst in phosphate buffer (PBS). Herein, we aimed to test this hypothesis and understand how an incorporated structural element side chain affects WO. To this aim, we prepared a set of peptoid trimers each with a different structural element replacing the benzyl group by either naphthyl, cyclohexyl, benzyl, propyl chloride, or propyl side chains as well as a peptoid lacking a structural element. We studied the structure of their Cu complexes and tested these complexes as electrocatalysts for WO. We discovered that while all the peptoids self-assemble to form dinuclear Cu-peptoid complexes, the duplex that has no structural side chain, Cu_2(**BE**)$_2$, is structurally different from the others in the solid state. Moreover, Cu_2(**BE**)$_2$ remains dinuclear in a PBS at pH 11, while all the other duplexes are mononuclear in the PBS. Finally, though most of the complexes showed low electrocatalytic activity for WO, the dinuclear complex Cu_2(**BE**)$_2$ performed with the highest turnover frequency of 484 s^{-1}. Nevertheless, this dinuclear complex slowly decomposes to the corresponding mononuclear complex as a more stable species during WO, while the other mononuclear complexes retain their structure in solution but display much slower kinetics (ca. 5 to 8 s^{-1}) under the same conditions. Overall, our results demonstrate that bulkier side chains hamper the stability of dinuclear Cu-peptoids in a PBS, and hence, their efficiency as WO electrocatalysts is also hampered.

Keywords: copper; peptoid; mononuclear; dinuclear; self-assembly; water oxidation; electrocatalysis; homogeneous

Citation: Ruan, G.; Fridman, N.; Maayan, G. Structure–Function Relationship within Cu-Peptoid Electrocatalysts for Water Oxidation. *Inorganics* **2023**, *11*, 312. https://doi.org/10.3390/inorganics11070312

Academic Editors: Gary Brudvig and Ning Yan

Received: 12 July 2023
Revised: 20 July 2023
Accepted: 21 July 2023
Published: 24 July 2023

1. Introduction

Remarkable progress in the development of earth-abundant-metal-based water oxidation catalysts has been made over the last two decades [1–4], and electrocatalytic water oxidation (WO) has become a potent strategy for producing hydrogen gas as a renewable energy source and green fuel [5–10]. Yet, the poor thermodynamic driving force, i.e., overpotential, of WO requires a profound understanding of the molecular scale in order to overcome it [11–13]. Studies of molecular catalysts and homogeneous catalytic reactions are used to reveal insights for improving reaction efficiency [14–16]. In particular, their well-defined structures can be precisely tailored to gain more knowledge of how to develop efficient electrocatalysts for WO [17–20]. This includes the study of weak-bonding interactions, electronic inductive and conjugative effects, steric hindrance, self-assembly, and more [21–29].

Pioneering research from 2012 shed light on the high-rate kinetics of $Cu(BPy)(OH)_2$ (BPy = 2,2′-bipyridine) as the first Cu-based homogeneous WO catalyst. Since then, numerous small-molecule-based Cu-BPy or Cu-polypyridyl WO catalysts have been reported [30–48]. Apart from them, Cu-peptide-based WO electrocatalysts, which are inspired by the natural Cu-oxygen active species in enzyme environments, have also been developed, and they exhibit relatively low overpotentials [49–55]. However, a drawback of using peptides as ligands is that the metal binding is pH-dependent due to the pKa value of the N-H in amide bonds, which is also susceptible to oxidation, and therefore they have low stability [56–58]. To address this issue, peptoids, N-substituted glycine oligomers [59,60], were developed as metal chelators [61–71] and biomimetic catalysts [72–77]. In addition to their stability toward various pH and oxidation conditions, peptoids are highly versatile as innumerable primary amines can be incorporated as functional side chains or structural elements, making the peptoid sequence and structure also tunable [78–80]. Recent work from our laboratory introduced **BEBenzyl**, a peptoid trimer having the side chains BPy (**B**) and hydroxyl (**E**) and a benzyl group as a structural element, which forms a Cu-peptoid complex as an efficient homogeneous WO electrocatalyst [74]. After complexation with a Cu salt, a self-assembled dinuclear Cu architecture (Cu:peptoid = 2:2, mode I in Scheme 1) is generated [81]. Interestingly, it decomposes into mononuclear (Cu:peptoid = 1:1, Cu**BEBenzyl**) once the solution environment is changed from pure water to 0.1 M phosphate buffer at pH 11~11.5, in which it can be used for electrocatalytic WO [74]. DFT calculations suggested that the benzyl side chain structurally directs the hydroxyl side chain to bind the Cu center, assisting in stabilizing the high-oxidation state intermediates during WO. However, this hypothesis was not examined experimentally.

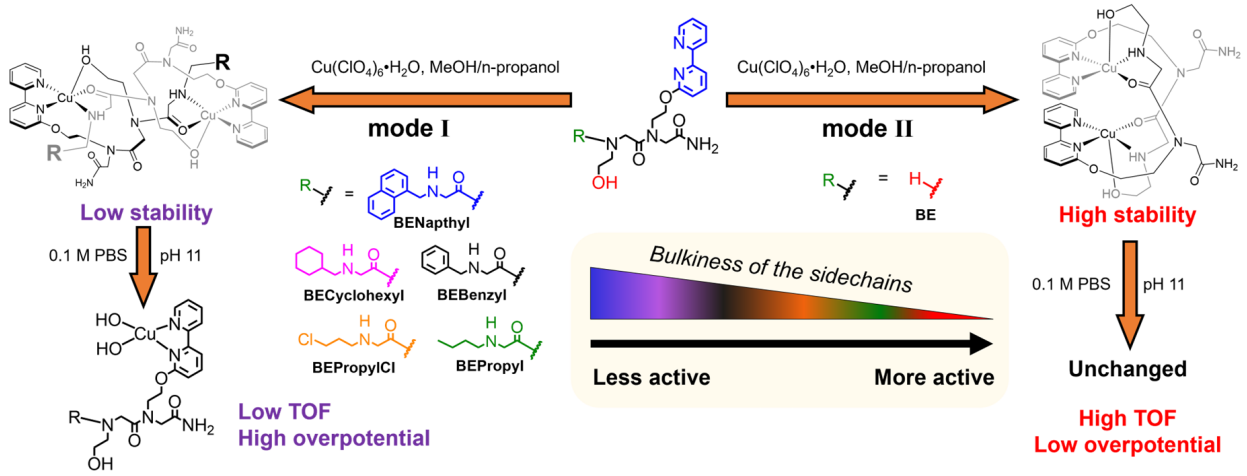

Scheme 1. Summary of the self-assembled Cu-peptoids studied in this work and their WO activity.

To test this hypothesis and understand how a structural element affects WO, we replaced the benzyl group with either naphthyl, cyclohexyl, benzyl, propyl chloride, or propyl side chains forming a set of peptoid trimers, each with a different structural element, namely **BENapthyl**, **BECyclohexyl**, **BEBenzyl**, **BEPropylCl**, or **BEPropyl**, or eliminated the benzyl group side chain to form the peptoid **BE**, which lacks a structural element. This set of peptoids underwent complexation with $Cu(ClO_4)_2{\cdot}6H_2O$, the newly formed complexes were recrystallized, their structures were characterized both in the solid state and in a phosphate buffer solution (PBS) at pH 11, the media in which electrocatalytic WO was studied, and their ability to perform as WO electrocatalysts in these conditions was examined. We discovered that upon Cu binding, all the trimers self-assembled into di-Cu-peptoid complexes having one type of architecture, "mode I", which dissociated in the PBS at pH 11 to the mononuclear complexes, which show poor WO electrocatalytic activity (Figure 1). In contrast, the dimer **BE** formed the complex $Cu_2(\mathbf{BE})_2$ in a different type of architecture, "mode I", which is stable in a PBS at pH 11. In these conditions, it

is an efficient electrocatalyst for WO, performing with the lowest overpotential and with a 100-fold higher turnover frequency (TOF) compared with the mononuclear complexes tested in this study. These results suggest that the structural element side chain does affect the electrocatalytic performance in WO but hampers it rather than facilitating it.

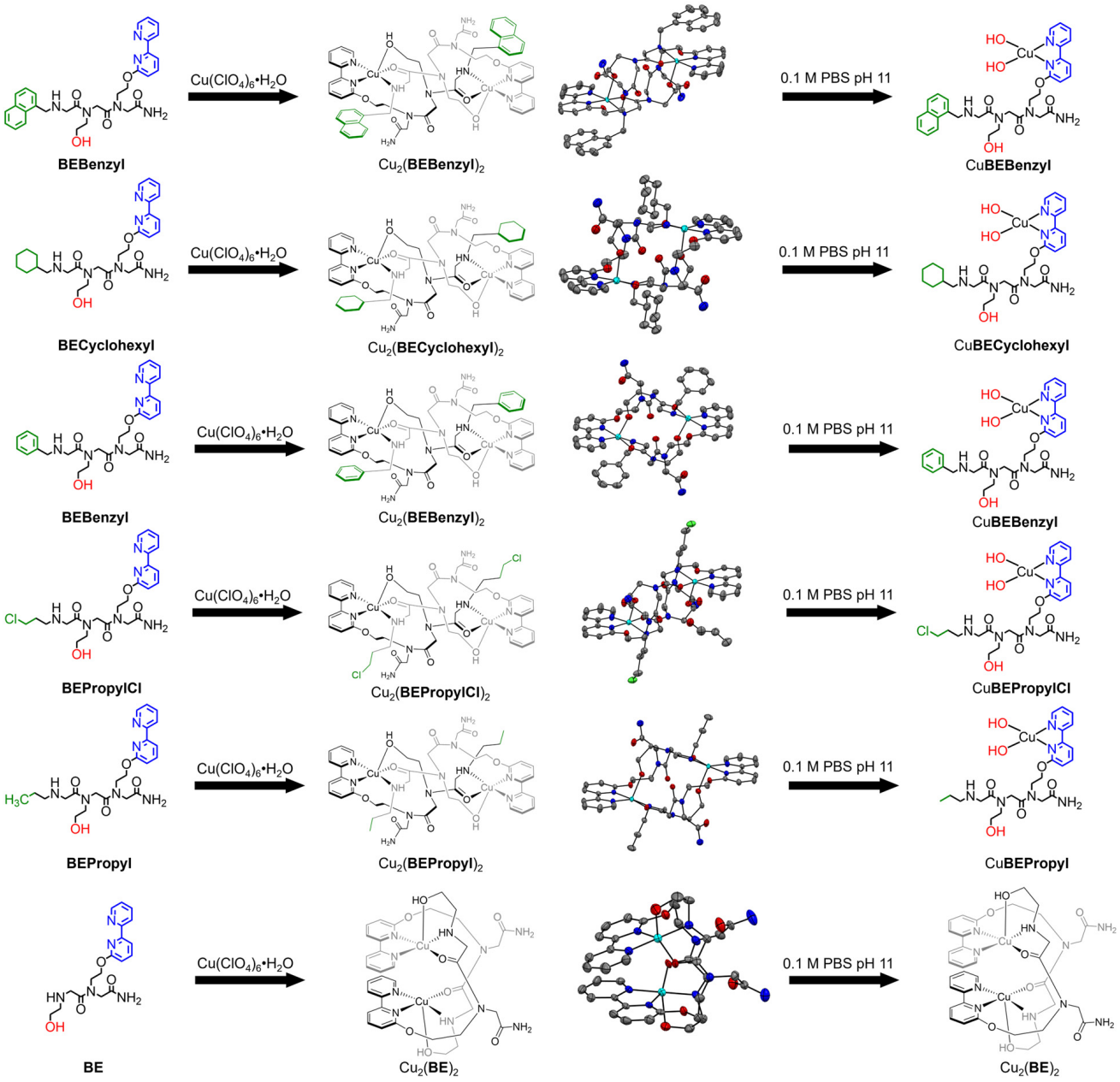

Figure 1. Molecular structures and ORTEP views (thermal ellipsoids set at 50% probability) of peptoids, corresponding self-assembled dinuclear architectures, and the complexes in 0.1 M PBS at pH 11. For crystal structures, the counter anions and hydrogen atoms are omitted for clarity. Gray: C; blue: N; red: O; green: Cl; cyan: Cu. Bond lengths and angles are listed in supporting information.

2. Results and Discussion

2.1. Structural Characterization of Cu-peptoid Complexes in 0.1 M PBS pH 11

All the peptoids described in this study were synthesized using the submonomer solid-phase method [60], cleaved from the solid support, and purified by high-performance liquid chromatography (HPLC, >95% purity) (Figures S1–S3). The molecular weights measured by electrospray mass spectrometry (ESI–MS) were consistent with the calculated mass for the corresponding sequences (Figures S4–S6). The corresponding data of **BENapthyl**, **BEBenzyl**, and **BE** have been reported [77,81,82]. The purified peptoids were treated with 1 equiv. of $Cu(ClO_4)_2 \cdot 6H_2O$ in methanol or n-propanol, and after 4 h of stirring, greenish-blue or blue precipitates were expected to be obtained. The precipitated solids were isolated and washed three times. The remaining solids were further dried and recrystallized in specific solvent environments (details in Section 3.3). Among them, the characterizations and crystal structural details of Cu_2(**BE**)$_2$, Cu_2(**BEBenzyl**)$_2$, and Cu_2(**BENapthyl**)$_2$ have been reported recently from our laboratory [77,81,82]. The new solid structures of Cu_2(**BECyclohexyl**)$_2$, Cu_2(**BEPropylCl**)$_2$, and Cu_2(**BEPropyl**)$_2$ were characterized by X-ray crystallography (CCDC number: 2253528, 2253526, and 2253527, respectively). The structure of these complexes resembles the structures of Cu_2(**BEBenzyl**)$_2$ and Cu_2(**BENapthyl**)$_2$, which showed centrosymmetric self-assembled architectures (Figures S7–S9): each Cu^{II} is penta-coordinated and adopts a distorted square-pyramidal geometry [81]. The two BPy N atoms from one peptoid ligand and the carbonyl O atom (C=O) and terminal N atom (NH) from the other peptoid ligand construct the equatorial square base of each Cu^{2+} center, while the O atom (OH) of the ethanolic side chain occupies the apical position of the pyramid. We defined these structures as "mode I" self-assemblies. In mode I, the intramolecular cooperative interaction between the two Cu^{II} centers seems impossible because both pyramid-like coordination geometries are separated from each other, and the distance Cu···Cu is 6.757~6.921 Å. On the contrary, the structure of Cu_2(**BE**)$_2$, defined here as "mode II" self-assembly, is different; the two bipyridine groups are on the same side of the assembly, and the distance between the two Cu ions is much shorter—only 4.270 Å. Therefore, Cu_2(**BE**)$_2$ is likely to bridge a H_2O (or OH^- in basic conditions) molecule to perform cooperative interaction between two Cu^{II} centers [77]. Although each Cu^{II} is penta-coordinated with the same atoms from the peptoid ligand and adopts a distorted square-pyramidal geometry, in mode I, the equatorial planes of Cu^{II} centers face each other with an offset π-π interaction between two BPy groups (3.246~3.396 Å) (Table 1) [83–86]. Apart from the solid state, all the prepared Cu-peptoids were also characterized as dinuclear complexes in a pure water solvent by ESI-MS and UV-Vis (Figures S10–S21).

Table 1. Summary of structure–function relationships of a series of designed Cu-peptoid complexes toward electrocatalytic water oxidation.

Complex [a]	Solid State or in Pure Water	Cu···Cu Distance in Dinuclear Form	In 0.1 M PBS (pH 11)	TOF (s^{-1})	Onset Potential (V vs. NHE)
Cu**BENapthyl**	Dinuclear (mode I)	6.787 Å	Mononuclear	5.2	+1.26
Cu**BECyclohexyl**	Dinuclear (mode I)	6.757 Å	Mononuclear	5.3	+1.26
Cu**BEBenzyl**	Dinuclear (mode I)	6.805 Å	Mononuclear	5.8	+1.24
Cu**BEPropylCl**	Dinuclear (mode I)	6.912 Å	Mononuclear	6.1	+1.20
Cu**BEPropyl**	Dinuclear (mode I)	6.921 Å	Mononuclear	7.7	+1.18
Cu_2(**BE**)$_2$	Dinuclear (mode II)	4.270 Å	Dinuclear (mode II)	484 (43) [b]	+1.08

a: the order of the entry is following the bulkiness of the structural elements, from napthyl to none (-H); b: this value is calculated after pH adjustment following 2 h CPE.

All Cu-peptoid complexes were further characterized in a PBS at pH 11. ESI-MS showed the mass signals representing the corresponding mononuclear complexes (Cu:peptoid = 1:1) Cu**BENapthyl**, Cu**BECyclohexyl**, Cu**BEBenzyl**, Cu**BEPropylCl**, and Cu**BEPropyl** at 667.7 m/z,

623.7 m/z, 617.6 m/z, 603.7 m/z, and 569.8 m/z in a 0.1 M PBS at pH 11 (Figures S22–S26). The mass signals for the self-assembled complexes (Cu:peptoid = 2:2) were not observed except for Cu_2(**BE**)$_2$ (Figure S27). The instability of the dinuclear self-assembled Cu-peptoids in a PBS at pH 11 compared to their stability in pure water was also observed in the comparison of UV-Vis absorbance bands of the complexes in each solvent. While in pure water, the spectrum showed absorbance bands near 320 nm and 248 nm, indicating the presence of the intact self-assembled dinuclear Cu-peptoid complexes, in a PBS at pH 11, these two bands are not present, and instead, two new absorbance bands near 300 nm and 236 nm appear, indicating a significant structural change (Figures S28–S32). These results support the results from the MS, suggesting that the self-assembled complexes are not stable in a PBS at pH 11. Interestingly, only the UV-Vis spectrum of Cu_2(**BE**)$_2$ showed absorbance bands near 320 nm and 248 nm, and no other bands were observed, suggesting that this dinuclear Cu-peptoid complex is stable in a PBS at pH 11 (Figure S33). These results suggest that the structural element has a key role not only in the self-assembly of the peptoids upon Cu binding and in the final structure of the dinuclear Cu-peptoid complexes but also in the stability of these complexes in a PBS at pH 11. Thus, when the peptoid sequence includes a structural element as a side chain, the peptoids are self-assembled upon Cu binding to one type of structure (mode I, Figure 1), which is instable in a PBS at pH 11, where it dissociates to the monomeric Cu-peptoid complex, while the peptoid dimer that does not include a structural element side chain self-assembles upon Cu binding to a second type of structure (mode II, Figure 1), which is maintained in a PBS pH 11.

2.2. Electrocatalytic Activities of the Cu-Peptoid Complexes in PBS toward Water Oxidation

2.2.1. Electrochemical Properties

The electrochemical properties of the complexes in a 0.1 M PBS at pH 11 were examined for WO. The cyclic voltammetry (CV) and differential pulse voltammetry (DPV) were probed under air using a glassy carbon (GC) working electrode and a Ag/AgCl reference electrode. All the potential values are transferred and reported versus the normal hydrogen electrode (vs. NHE). Each complex (0.5 mM based on the molecular weight of mononuclear Cu-peptoids, unless noted differently) was dissolved in a 0.1 M PBS at pH 11, and its CV was measured. In the scanning window between 0 and +0.4 V (Figure S34), an oxidation wave was observed consistent with Cu^I to Cu^{II} [87–89]. However, the CV scan of Cu_2(**BE**)$_2$ in the same oxidation window showed an oxidation potential of E_p = +0.15 V, which is broader, suggesting that more than one electron transfer is taking place at this potential (consistent with the existence of two Cu centers in this complex) [31,32,77] and about 120 mV lower than those of the mononuclear complexes (for Cu**BECyclohexyl**, Cu**BEPropylCl**, and Cu**BEPropyl**, E_p = +0.27 V, and for Cu**BENapthyl**, E_p = +0.29 V). These differences are rationally relevant to their structural divergence (di- vs. mononuclear). Extending the scanning window up to +1.5 V, the CV scans of all the mononuclear complexes showed a broad irreversible oxidation wave E_p from +1.40 V to +1.30 V, with the Cu**BENapthyl** showing the highest potential, thereafter Cu**BECyclohexyl**, Cu**BEBenzyl**, Cu**BEPropylCl**, and finally Cu**BEPropyl** showing the lowest oxidation potential (Figure 2a). This cathodic shift in both CVs and DPVs (Figure S35) matches the order of the bulkiness of the structural element side chains, which are from the bulkiest to the least bulky. Notwithstanding this, these oxidation currents of the mononuclear complexes remain similar (i_p = ca. 18 μA). In the same potential window, at E_p = +1.36 V, the irreversible oxidation of Cu_2(**BE**)$_2$ reveals that the corresponding current intensity increases up to 155 μA, which is nearly 9-fold higher than that of the mononuclear complexes (Figure 2b). This irreversible oxidation is recognized as a catalytic event and a typical curve representing the EC mechanism observed in the plots of normalized current vs. scan rates (Figure S36) [90].

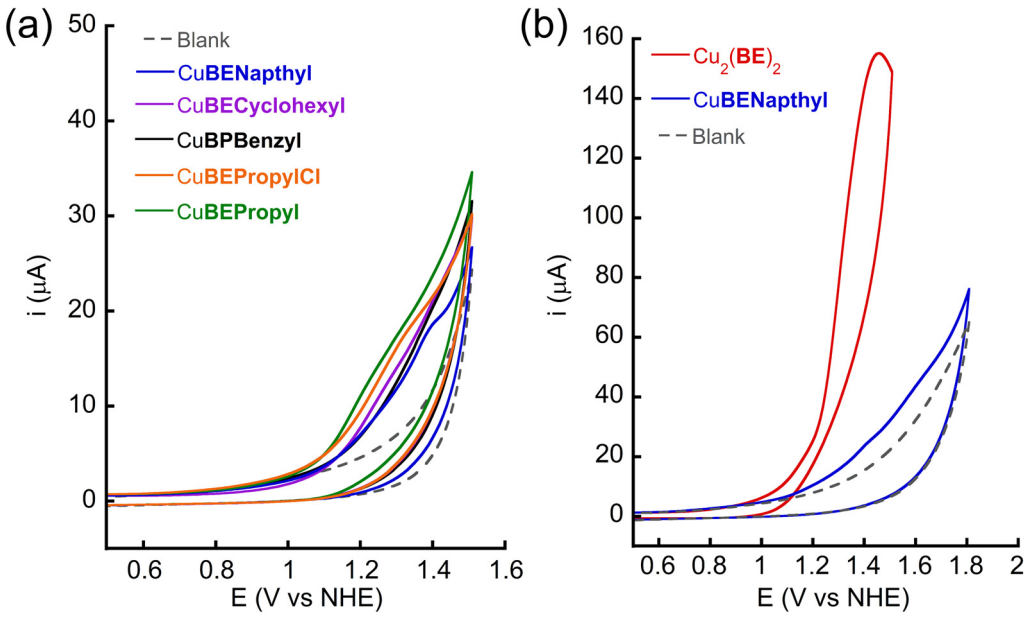

Figure 2. (**a**) CVs of 0.1 M phosphate buffer solution at pH 11 in the absence (gray dash line) or presence of 0.5 mM Cu**BENapthyl**, Cu**BECyclohexyl**, Cu**BEBenzyl**, Cu**BEPropylCl**, and Cu**BEPropyl**. (**b**) CVs of 0.1 M phosphate buffer solution at pH 11 in the absence (gray dash line) or presence of 0.5 mM Cu**BENapthyl** or Cu_2(**BE**)$_2$ (according to the molecular weight of dinuclear complex). Scan rate = 100 mV/s, glassy carbon electrode as the working electrode.

2.2.2. Kinetics Studies

The CV results suggest that Cu_2(**BE**)$_2$ is a much more efficient electrocatalyst for WO than the mononuclear complexes. The rate constant (k_{obs}), known as TOF, is a significant parameter for quantifying the efficiency of WO electrocatalysts [91,92]. To calculate the k_{obs}, of all the Cu-peptoid complexes, a series of CVs at different scan rates (Figure S37) using Cu_2(**BE**)$_2$ or Cu**BENapthyl** were examined and applied to foot-of-the-wave analysis (FOWA), which represents the intrinsic TOF at zero overpotential [93]. This method was selected also to be consistent with our previous studies [74] in order to enable comparison of the obtained values. To calculate the TOF, we followed the equation shown as follows in Equation (1), where i_{cat} is the catalytic current of the catalyst, i_p is the oxidative wave of Cu^{II}/Cu^{I} (Figure S37) as the approximated diffusion current, R is the universal gas constant, T is the absolute temperature, F is the Faraday constant, ν is the scan rate, E_{cat} is the catalytic potential, and E is the applied potential. i_{cat}/i_p vs. $1/(1 + \exp[(F/RT)(E_{cat} - E)])$ was plotted, and a straight line could be obtained, where the k_{obs} could be calculated according to the linear slope (Figures 3a and S38) [94–96].

$$\frac{i_{cat}}{i_p} = \frac{2.24n\sqrt{\frac{RTk_{obs}}{Fv}}}{1 + \exp\left[\frac{F}{RT}(E_{cat} - E)\right]} \quad (1)$$

Subsequently, the k_{obs} (TOF) values of Cu_2(**BE**)$_2$ and Cu**BENapthyl** were calculated to be 484 s^{-1} and 5.2 s^{-1}, respectively (Figure 3b). Notably, the TOF of Cu**BENapthyl** is consistent with that of Cu**BEBenzyl**, previously calculated at pH 11.5 which is 5.8 s^{-1} [74], while the TOF of Cu_2(**BE**)$_2$ is almost 100-fold higher than that of Cu**BENapthyl**, as well as Cu**BEBenzyl**. As the concentration of Cu centers in Cu_2(**BE**)$_2$ is double the concentration of Cu centers in Cu**BENapthyl**, but the TOF is 100-fold higher rather than 2-fold higher, we suggest that there might be some cooperativity between the two Cu centers in Cu_2(**BE**)$_2$ that is playing a key role in enhancing the kinetic rate of WO [34,77,97–99].

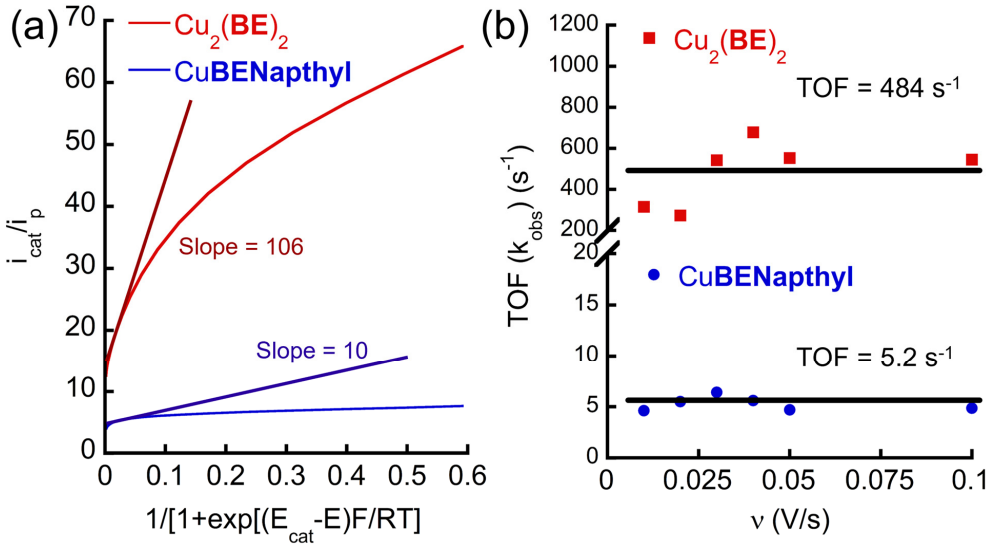

Figure 3. (**a**) The experimental data of CVs of Cu_2(**BE**)$_2$ and Cu**BENapthyl** in 0.1 M PBS at pH 11 used for FOWA at scan rate 100 mV/s. The straight lines represent the fitting line to calculate the TOF with corresponding slope values. (**b**) The TOF values of Cu_2(**BE**)$_2$ and Cu**BENapthyl** were calculated by FOWA at various scan rates. The horizontal lines represent the overall average TOF values.

2.2.3. Electrocatalytic Water Oxidation and Homogeneity Studies

As Cu_2(**BE**)$_2$ had a high TOF toward WO, it was subjected to a controlled potential electrolysis (CPE) experiment applying a constant potential of E = +1.25 V using 0.5 mM Cu_2(**BE**)$_2$ in a 0.1 M PBS at pH 11 using ITO as working electrode (Figures 4 and S39). After 2 h of the CPE experiment, 7.32 C of charge was accumulated, and 19 µmol of O_2 was probed with an oxygen sensor. Subtracted by the amount of oxygen (1 µmol) and charge (0.26 C) accumulated within 2 h of CPE in the absence of a catalyst, a Faradaic efficiency (FE%) of 98% was calculated. Despite this high FE%, the current density dropped slowly from about 2.2 mA/cm^2 to 0.22 mA/cm^2 within 2 h, which indicates either the instability of the catalyst or the influence of the pH change (from 11.0 to 9.5) during the reaction. UV-Vis analysis of the catalyst before and after CPE showed that the absorbance bands near 320 nm and 248 nm shifted to 305 nm and 239 nm in UV-Vis spectroscopy, respectively (Figure S40). More importantly, the catalytic wave at E_p = +1.36 V disappeared, and only the peak at E_p = +1.43 V was obtained (Figure S41). Re-adjusting the pH back to 11 did not lead to the recovery of the catalytic oxidative wave at E_p = +1.36 V (Figure S41). Moreover, the current density was 0.30 mA/cm^2 during the entire CPE experiment, which is similar to the current density obtained after the 2 h CPE experiment using Cu_2(**BE**)$_2$ before pH adjustment (0.22 mA/cm^2), excluding the possibility that the decay of the current density was attributed to pH change (Figure 4). These results indicate that Cu_2(**BE**)$_2$ is capable of catalyzing WO at a high current density, consistent with the calculated TOF, and indicating a fast kinetic rate in these conditions (Figure 3). However, slow decay of the kinetic rate occurred during electrolysis leading to a sharp decrease in the TOF from 484 s^{-1} to 43 s^{-1} (after adjusting pH), implying that Cu_2(**BE**)$_2$ decomposes during the WO reaction.

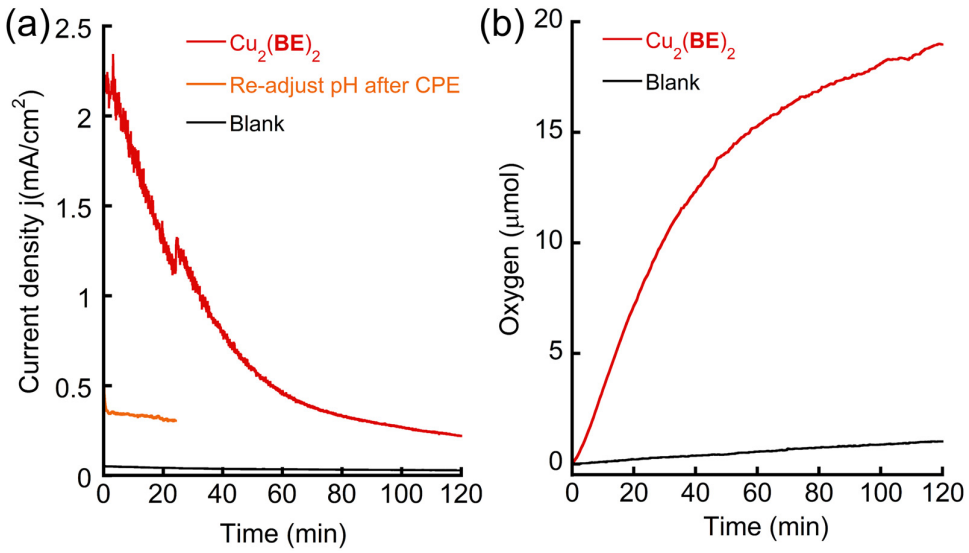

Figure 4. (**a**) Current density j, and (**b**) oxygen evolution of the CPE experiments using 0.5 mM Cu_2(**BE**)$_2$ or without any catalyst as blank in 0.1 M PBS at pH 11 using ITO as working electrode at applied potential +1.25 V vs. NHE. The orange curve represents another CPE of the same solution responsive to the red curve but with re-adjusted pH from 9.5 to 11.

The instability of Cu_2(**BE**)$_2$ can be attributed to the following: (1) its decomposition on the working electrode surface, forming less active or inactive heterogeneous species, or (2) its decomposition to a different, less active (or inactive) homogeneous species in the solution during electrocatalysis. To probe the homogeneity of Cu_2(**BE**)$_2$ in the reaction, we carried out 10 continuous CV scans from +0.4 to +1.5 V in a solution [100]. Interestingly, the catalytic peak significantly decreased during these scans, and the intensity of the last scan was similar to that obtained in the CV scans performed after CPE (Figure S42). The glassy carbon working electrode was then removed from the solution and rinsed with deionized water (the electrode was not polished), then placed in a fresh 0.1 M PBS without Cu_2(**BE**)$_2$. The CV scan of this solution showed only the buffer response (Figure S43). In other words, no active species was formed on the surface of the working electrode. To clearly observe the electrode surface, both the ITO working electrode after CPE for 2 h and a clean ITO electrode as control were analyzed by high-resolution scanning electron microscopy (HR-SEM) and energy-dispersive X-ray spectroscopy (EDX). No particles on the electrode's surface were found in HR-SEM (Figure S44), and no Cu element was found attached during EDS after electrolysis (Figure S45). Therefore, we can exclude assumption (1) and conclude that no heterogeneous process took place during electrocatalysis. Considering that the CV and UV-Vis analysis of Cu_2(**BE**)$_2$ after 2 h CPE was strikingly different from those performed before CPE, but akin to those of the fresh mononuclear complexes, assumption (2) is probable. To probe whether Cu_2(**BE**)$_2$ decomposes to its corresponding mononuclear complex during electrolysis, we tested the behavior of 1.0 mM Cu**BENapthyl** under CPE conditions, as well as the solution of 0.5 mM Cu_2(**BE**)$_2$ after 2 h CPE with re-adjusted pH. Both reactions were conducted at an applied potential of +1.4 V, which is near their catalytic oxidation peaks (Figure 5). The obtained current densities in both cases were below 0.5 mA/cm^2—strikingly lower than the current density obtained from the CPE catalyzed by fresh Cu_2(**BE**)$_2$, in which a 150 mV lower overpotential was applied (Figure 4). Collectively, the similarities in the analysis and catalytic properties between Cu**BENapthyl** and re-used Cu_2(**BE**)$_2$ strongly suggest that the self-assembled dinuclear Cu_2(**BE**)$_2$ complex, although stable in a PBS at pH 11, decomposes to the more stable corresponding mononuclear complex during electrocatalytic WO.

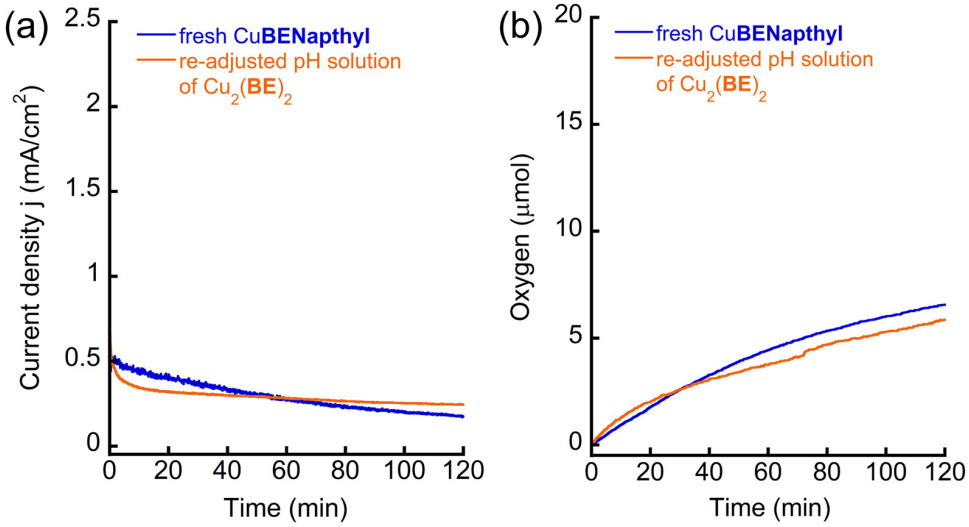

Figure 5. (**a**) Current density, j, and (**b**) oxygen evolution of the CPE experiments of 1.0 mM Cu**BENapthyl** or solution containing Cu_2(**BE**)$_2$ in which the pH was re-adjusted after previous CPE at +1.25 V, in 0.1 M PBS at pH 11 using ITO as working electrode at applied potential +1.4 V vs. NHE.

2.3. Structure–Function Relationship

The structural and electrocatalytic performances toward the WO of all six complexes involved in this study are summarized in Table 1. From this table, it is clear that (1) all the Cu-peptoid complexes, self-assembled in both mode I and mode II to dinuclear structures, are stable both in the solid state and in pure water; (2) all the dinuclear complexes self-assembled in mode I decompose to a mononuclear complex in a 0.1 M PBS at pH 11, while Cu_2(**BE**)$_2$, self-assembled in mode II, is also stable in these conditions; (3) the kinetics (TOF) of Cu_2(**BE**)$_2$ are much faster than those of the mononuclear complexes, and among the mononuclear ones, the TOF value gets higher when the incorporated structural element is less bulky; and (4) the thermodynamic requirement (onset potential) for Cu_2(**BE**)$_2$ to catalyze WO is lower than that required for the mononuclear complexes—among them, this value becomes lower when the incorporated structural element is less bulky. Therefore, we can conclude that the dinuclear complex Cu_2(**BE**)$_2$ is a much more efficient WO electrocatalyst than the mononuclear complexes in the same conditions. Similar observations and conclusions are also supported in other catalyst studies and are detailed in Table 2. However, it is unstable and loses its activity in 2 h of CPE because it decomposes to the mononuclear complex during water oxidation in a 0.1 M PBS at pH 11.

Table 2. Summary and comparison of WO performance with reported dinuclear vs. mononuclear catalysts.

Complex [a]	Nuclearity	Onset Potential (V vs. NHE) [a]	TOF (s^{-1})	Reference
Cu_2(**BE**)$_2$	Dinuclear	+1.08	484 (43) [b]	This work
Cu**BENapthyl**	Mononuclear	+1.26	5.2	
TNC-Cu	Trinuclear	~+1.6 *	20,000	[34] [b]
$HappCu_2$	Dinuclear	~+1.65 *	1375	
$F\text{-}N_2O_2Cu$	Mononuclear	~+1.85 *	131.6	
cat 1	Dinuclear	~+1.25 *	144	[97] [c]
cat 2	Mononuclear	~+1.35 *	4.86	
Fe(dpa)	Dinuclear	~+1.2 *	2.2	[101] [d]
Fe(ppq)	Mononuclear	~+1.4 *	0.23	
TNC-Ni3	Trinuclear	+1.24	0.54	[102] [e]
TNC-Ni2	Dinuclear	~+1.44 *	0.02	

(a): the onset potential values with symbol "*" are measured roughly; the electrochemical studies are performed in (b) 1.0 M NaHCO3 at pH 8.4, (c) 0.1 M PBS at pH 12, (d) 0.1 M nitric acid buffer at pH 1, (e) 0.1 M PBS at pH 7.

The efficiency of the Cu-peptoid catalysts highly depends on their structures in the WO condition. We suggest that the ability of Cu_2(**BE**)$_2$ to maintain the self-assembled dinuclear complex in a 0.1 PBS at pH 11 is attributed to the offset π-π interaction of two Bipy ligands from the two peptoid ligands in mode II [83–86] and to the short Cu···Cu distance (4.270 Å) that allows the two penta-coordinated Cu^{II} to coordinate to the μ-OH anion bridge from the basic solution [31,77,96,103]. Having a structural element within their sequences, the self-assembled duplexes in mode I lack this π-π stacking between the two BPy ligands located opposite to each other. Instead, they might prefer to coordinate OH^- individually, leading to the formation of mononuclear complexes with two coordinated OH^-.

3. Materials and Methods

3.1. Materials

Rink Amide resin was purchased from Novabiochem; ethanolamine and 6-bromo-2,2′-bipyridine were purchased from Acros organics, Israel; N,N′-diisopropylcarbodiimide (DIC) and bromoacetic acid were purchased from Sigma Aldrich. The other chemicals used in this work were purchased from commercial sources and used without additional purification. 2-(2,2′-bipyridine-6-yloxy) ethylamine (**B**) was prepared according to a literature method [62], and –OH (**E**) group of ethanolamine was protected using a reported procedure [77]. The used solvents were of HPLC grade. High-purity deionized water was obtained by passing distilled water through a nanopore Milli-Q water purification system. Aqueous basic buffer solutions at pH 11 were prepared using specific concentrations of sodium dihydrogen phosphate and disodium hydrogen phosphate with added 0.1 M NaOH or HCl solution such that the final ionic strength equaled 0.1 M.

3.2. Instrumentation

Peptoid oligomers were analyzed by reversed-phase HPLC (analytical C18 column, 5 μm, 100 Å, 2.0 × 50 mm) on a Jasco UV-2075 instrument. A linear gradient of 5–95% ACN in water (0.1% TFA) over 10 min was used at a flow rate of 0.7 mL/min. Preparative HPLC was performed using a Phenomenex C18 column (15 μm, 100 Å 21.20 × 100 mm) on a Jasco UV-2075 instrument. Peaks were eluted with a linear gradient of 5–95% ACN in water (0.1% TFA) over 60 min at a flow rate of 5 mL/min. Mass spectrometry for peptoids and Cu-peptoid complexes was performed on a Waters LCT Premier mass and Advion expression mass under electrospray ionization (ESI), direct probe ACN:H2O (70:30), flow rate 0.2 mL/min. UV-Vis measurements were recorded on an Agilent Technologies Cary 60 UV-Vis spectrophotometer using a 1 cm path-length quartz cuvette. For high-resolution scanning electron microscopy (HR-SEM) imaging we used a Zeiss Ultra Plus high-resolution SEM, equipped with a Schottky field-emission gun. Specimens were imaged at low acceleration voltages of 1 kV and working distances of approx. 4 mm. We used the Everhart Thornley ("SE2") secondary electron imaging detector. For confirmation of sample composition, we used a Quantax energy-dispersive X-ray spectrometer (EDS, Bruker) at an acceleration voltage of 10 kV.

3.3. Synthesis of Cu-peptoids

The peptoid (0.1 mmol) was dissolved in 1 mL methanol (**BEBenzyl**, **BENapthyl**, or **BE**) or 1 mL 1-propanol (**BECyclohexyl**, **BEPropylCl**, or **BEPropyl**), and the mixture was stirred for 10 min. This mixture was treated with copper perchlorate hexahydrate (0.1 mmol as solid) and stirred for 4 h. A greenish-blue solid precipitate was obtained and was isolated by centrifugation, washed three times with corresponding methanol or 1-propanol, and dried in vacuum overnight. Then, the solid compounds were dissolved in specific mixed salts and solvents for crystallization at room temperature: blue crystal Cu_2(**BECyclohexyl**)$_2$ was obtained from slow evaporation of ACN/1-propanol with adding 2 equiv. ammonium hexafluorophosphate; blue crystal Cu_2(**BEPropylCl**)$_2$ was obtained from slow evaporation of ACN/1-propanol; blue crystal Cu_2(**Propyl**)$_2$ was obtained from

slow evaporation of ACN/1-propanol; Cu_2(**BEBenzyl**)$_2$, Cu_2(**BENapthyl**)$_2$, and Cu_2(**BE**)$_2$ were reported previously from our laboratory.

3.4. Electrochemical Methods

Cyclic voltammetry (CV) and differential pulse voltammetry (DPV) experiments were carried out on an EmStat3 potentiostat. Solutions of the complexes were placed in one-compartment three-electrode cells. Glassy carbon (GC) was used as a working electrode, Ag/AgCl as a reference electrode, and Pt wire as a counter electrode. Working electrode pretreatment before each measurement included polishing with 0.05 μm alumina paste, followed by rinsing with water, and finally drying in air. All potentials in the present work are reported versus NHE by adding 0.20 V to the measured potential (Ag/AgCl vs. NHE). CVs were collected at 100 mV/s, except for other specifications. DPV was obtained with following parameters: amplitude = 200 mV, E-step = 10 mV, pulse width = 0.02 s.

3.5. Oxygen Evolution Experiments

Controlled potential experiments (CPEs) were performed using a two-compartment cell closed with septum. Large-surface porous carbon (spongy shape) as working electrode together with an Ag/AgCl (NaCl sat.) as reference electrode were placed in one of the compartments that was filled with buffer solution containing certain concentration of catalyst (0.1 M PBS at pH 11). In the other compartment, containing only the fresh buffer solution, a mesh platinum counter electrode was used. Before starting the experiment, nitrogen gas was purged for 10 min to remove the oxygen from the system. Oxygen evolution was monitored in the gas phase with a Fixed Needle-Type Oxygen Minisensor (from PyroScience) placed in the headspace of the reaction vassal (working electrode side). The CPE started as soon as the oxygen sensor signal was stable. During the experiment, solutions of both compartments were vigorously stirred. The results of the water oxidation catalysis with copper complex were compared with the blank experiment in the same conditions but in the absence of the catalyst. The Faraday efficiency was determined according to the total charge passed during the CPE and the total amount of generated oxygen as a four-electron oxidation process. The oxygen was measured with the oxygen sensor in % and converted to μmol using a calibration curve. This was constructed by the gradual addition of the known amount of pure oxygen (μL) into the cell containing buffer solution using a Hamilton syringe while measuring the oxygen in % by the oxygen sensor and then by plotting the amount of pure oxygen added (μL) vs. the amount of oxygen (%) shown by oxygen sensor to get the total amount of oxygen evolved in μL during electrolysis (Figure S46). This was further converted to μmol via the following equation: y μmol = x μL/(24.5 L/mol), T = 298 K. Faradaic efficiency (FE%) was calculated using following equation: FE% = n_{O_2}/(Q/nF) * 100%, where n_{O_2} is the mole of oxygen from CPE experiment, mol; Q is accumulated charge from CPE experiment, C; n is the number of electrons transferred, 4; and F is Faraday constant, 96,485 C/mol.

4. Conclusions

In conclusion, we designed and characterized six Cu-peptoid complexes: five with structural elements, Cu_2(**BENapthyl**)$_2$, Cu_2(**BECyclohexyl**)$_2$, Cu_2(**BEBenzyl**)$_2$, Cu_2(**BEPropylCl**)$_2$, and Cu_2(**BEPropyl**)$_2$, which self-assemble in mode I, and one without introducing a structural element, Cu_2(**BE**)$_2$, which self-assembles in mode II. They are all stable as duplexes in the solid state and in pure water. However, the dinuclear structure Cu_2(**BE**)$_2$ is also stable in a 0.1 M PBS at pH 11, which are suitable conditions for WO, where the other dinuclear complexes decompose to their corresponding mononuclear complexes, Cu**BENapthyl**, Cu**BECyclohexyl**, Cu**BEBenzyl**, Cu**BEPropylCl**, and Cu**BEPropyl**, respectively, in these conditions. We suggest that a π-π stacking interaction and a short Cu···Cu distance enhance the stability of the dinuclear complex Cu_2(**BE**)$_2$ in basic conditions. Thus, in comparison to the mononuclear Cu-peptoids, Cu_2(**BE**)$_2$ is a much better electrocatalyst for WO, exhibiting a lower onset potential and a 100-fold faster TOF. Nevertheless, Cu_2(**BE**)$_2$ was shown to

slowly decompose to the mononuclear species during homogeneous WO, leading to a sharp decrease in its TOF. These results shed light on the benefits of using dinuclear catalysts with intrinsic cooperativity between the metal centers. Our results also demonstrate that an incorporated structural element has a key role in controlling the self-assembly mode (I or II) of the peptoid upon Cu binding, and the stability of the self-assembled complexes in a PBS at a basic pH. These sequence–structure–function relationships within Cu-peptoid electrocatalysts for WO should expand the molecular design of metallo-biomimetic oligomers as electrocatalysts for WO.

Supplementary Materials: The following supporting information can be downloaded at https://www.mdpi.com/article/10.3390/inorganics11070312/s1, Figures S1–S3: Analytical HPLC data of peptoid ligands, Figures S4–S6: ESI-MS data of peptoid ligands, Figures S7–S9: Crystal structures of Cu-peptoids, Figures S10–S15: ESI-MS data of Cu-peptoids in water, Figures S16–S21: UV-Vis data of Cu-peptoids in water, Figures S22–S27: ESI-MS data of Cu-peptoids in 0.1 M PBS at pH 11, Figures S28–S33: UV-Vis data of peptoids and corresponding Cu-peptoids in 0.1 M PBS at pH 11, Figure S34: CV data of Cu-peptoids with a scanning window from −0.4 to 0.6 V in 0.1 M PBS at pH 11, Figure S35: DPV data of Cu-peptoids in 0.1 M PBS at pH 11, Figure S36: Normalized CV data of Cu-peptoid, Figure S37: CVs with various scan rates of Cu-peptoids in 0.1 M PBS at pH 11, Figure S38: FOWA data of Cu-peptoid in 0.1 M PBS at pH 11, Figure S39: CPE data of Cu-peptoid in 0.1 M PBS at pH 11, Figures S40–S41: Characterization of the solution before and after CPE experiment, Figures S42–45: Homogeneity test data including CV, SEM, and EDX, Figure S46: Calibration curve for the measure of oxygen, Tables S1–S7: Structural information of Cu-peptoids including crystallography data, bond length, and angles.

Author Contributions: Conceptualization, G.R. and G.M.; methodology, G.R., N.F. and G.M.; software, G.R.; formal analysis, G.R. and N.F.; investigation, G.R.; data curation, G.R. and N.F.; writing—original draft preparation, G.R. and G.M.; writing—review and editing, G.R. and G.M.; project administration, G.M.; funding acquisition, G.M. All authors have read and agreed to the published version of the manuscript.

Funding: This research was funded by the Israel Ministry of Energy, grant number 221-11-090.

Institutional Review Board Statement: Not relevant.

Informed Consent Statement: Not applicable.

Data Availability Statement: CCDC numbers 2253526, 2253527, and 2253528 contain the supplementary crystallographic data for this paper. These data can be obtained free of charge from the Cambridge Crystallographic Data Center via www.ccdc.cam.ac.uk/data_request/cif (accessed on 11 July 2023).

Acknowledgments: The authors thank Yeshayahu Talmon and Inbal Weisbord from the Wolfson Department of Chemical Engineering for HR-SEM and EDX measurements and analysis.

Conflicts of Interest: The authors declare no competing financial interests.

References

1. Matheu, R.; Garrido-Barros, P.; Gil-Sepulcre, M.; Ertem, M.Z.; Sala, X.; Gimbert-Surinach, C.; Llobet, A. The development of molecular water oxidation catalysts. *Nat. Rev. Chem.* **2019**, *3*, 331–341. [CrossRef]
2. Chatenet, M.; Pollet, B.G.; Dekel, D.R.; Dionigi, F.; Deseure, J.; Millet, P.; Braatz, R.D.; Bazant, M.Z.; Eikerling, M.; Staffell, I.; et al. Water electrolysis: From textbook knowledge to the latest scientific strategies and industrial developments. *Chem. Soc. Rev.* **2022**, *51*, 4583–4762. [CrossRef]
3. Kondo, M.; Tatewaki, H.; Masaoka, S. Design of molecular water oxidation catalysts with earth-abundant metal ions. *Chem. Soc. Rev.* **2021**, *50*, 6790–6831. [CrossRef]
4. Chen, Q.F.; Guo, Y.H.; Yu, Y.H.; Zhang, M.T. Bioinspired molecular clusters for water oxidation. *Coord. Chem. Rev.* **2021**, *448*, 214164. [CrossRef]
5. Blakemore, J.D.; Crabtree, R.H.; Brudvig, G.W. Molecular Catalysts for Water Oxidation. *Chem. Rev.* **2015**, *115*, 12974–13005. [CrossRef]
6. Ardo, S.; Rivas, D.F.; Modestino, M.A.; Greiving, V.S.; Abdi, F.F.; Alarcon Llado, E.; Artero, V.; Ayers, K.; Battaglia, C.; Becker, J.P.; et al. Pathways to electrochemical solar-hydrogen technologies. *Energ. Env. Environ. Sci.* **2018**, *11*, 2768–2783. [CrossRef]

7. Kibsgaard, J.; Chorkendorff, I. Considerations for the scaling-up of water splitting catalysts. *Nat. Energy* **2019**, *4*, 430–433. [CrossRef]
8. Luque-Urrutia, J.A.; Ortiz-Garcia, T.; Sola, M.; Poater, A. Green Energy by Hydrogen Production from Water Splitting, Water Oxidation Catalysis and Acceptorless Dehydrogenative Coupling. *Inorganics* **2023**, *11*, 88. [CrossRef]
9. Chavan, H.S.; Lee, C.H.; Inamdar, A.I.; Han, J.; Park, S.; Cho, S.; Shreshta, N.K.; Lee, S.U.; Hou, B.; Im, H.; et al. Designing and Tuning the Electronic Structure of Nickel-Vanadium Layered Double Hydroxides for Highly Efficient Oxygen Evolution Electrocatalysis. *Acs Catal.* **2022**, *12*, 3821–3831. [CrossRef]
10. Inamdar, A.I.; Chavan, H.S.; Seok, J.H.; Lee, C.H.; Shin, G.; Park, S.; Yeon, S.; Cho, S.; Park, Y.; Shrestha, N.K.; et al. Optimal rule-of-thumb design of NiFeMo layered double hydroxide nanoflakes for highly efficient and durable overall water-splitting at large currents. *J. Mater. Chem. A* **2022**, *10*, 20497–20508. [CrossRef]
11. McEvoy, J.P.; Brudvig, G.W. Water-splitting chemistry of photosystem II. *Chem. Rev.* **2006**, *106*, 4455–4483. [CrossRef] [PubMed]
12. Hsu, W.C.; Wang, Y.H. Homogeneous Water Oxidation Catalyzed by First-Row Transition Metal Complexes: Unveiling the Relationship between Turnover Frequency and Reaction Overpotential. *Chemsuschem* **2022**, *15*, e202102378. [CrossRef] [PubMed]
13. Wang, M.; Wu, L.; Zhang, F.; Gao, L.L.; Geng, L.; Ge, J.B.; Tian, K.G.; Chai, H.; Niu, H.L.; Liu, Y.; et al. Doping with Rare Earth Elements and Loading Cocatalysts to Improve the Solar Water Splitting Performance of BiVO4. *Inorganics* **2023**, *11*, 203. [CrossRef]
14. Li, J.; Triana, C.A.; Wan, W.; Saseendran, D.P.A.; Zhao, Y.; Balaghi, S.E.; Heidari, S.; Patzke, G.R. Molecular and heterogeneous water oxidation catalysts: Recent progress and joint perspectives. *Chem. Soc. Rev.* **2021**, *50*, 2444–2485. [CrossRef]
15. Zhang, B.B.; Sun, L.C. Artificial photosynthesis: Opportunities and challenges of molecular catalysts. *Chem. Soc. Rev.* **2019**, *48*, 2216–2264. [CrossRef]
16. Francke, R.; Schille, B.; Roemelt, M. Homogeneously Catalyzed Electroreduction of Carbon Dioxide-Methods, Mechanisms, and Catalysts. *Chem. Rev.* **2018**, *118*, 4631–4701. [CrossRef]
17. Dau, H.; Limberg, C.; Reier, T.; Risch, M.; Roggan, S.; Strasser, P. The Mechanism of Water Oxidation: From Electrolysis via Homogeneous to Biological Catalysis. *Chemcatchem* **2010**, *2*, 724–761. [CrossRef]
18. Chalkley, M.J.; Garrido-Barros, P.; Peters, J.C. A molecular mediator for reductive concerted proton-electron transfers via electrocatalysis. *Science* **2020**, *369*, 850–854. [CrossRef]
19. Garrido-Barros, P.; Derosa, J.; Chalkley, M.J.; Peters, J.C. Tandem electrocatalytic N-2 fixation via proton-coupled electron transfer. *Nature* **2022**, *609*, 71–76. [CrossRef]
20. Nitopi, S.; Bertheussen, E.; Scott, S.B.; Liu, X.Y.; Engstfeld, A.K.; Horch, S.; Seger, B.; Stephens, I.E.L.; Chan, K.; Hahn, C.; et al. Progress and Perspectives of Electrochemical CO2 Reduction on Copper in Aqueous Electrolyte. *Chem. Rev.* **2019**, *119*, 7610–7672. [CrossRef]
21. Gil-Sepulcre, M.; Garrido-Barros, P.; Oldengott, J.; Funes-Ardoiz, I.; Bofill, R.; Sala, X.; Benet-Buchholz, J.; Llobet, A. Consecutive Ligand-Based Electron Transfer in New Molecular Copper-Based Water Oxidation Catalysts. *Angew. Chem. Int. Ed.* **2021**, *60*, 18639–18644. [CrossRef] [PubMed]
22. Matheu, R.; Ertem, M.Z.; Gimbert-Surinach, C.; Benet-Buchholz, J.; Sala, X.; Llobet, A. Hydrogen Bonding Rescues Overpotential in Seven-Coordinated Ru Water Oxidation Catalysts. *Acs Catal.* **2017**, *7*, 6525–6532. [CrossRef]
23. Wasylenko, D.J.; Ganesamoorthy, C.; Henderson, M.A.; Koivisto, B.D.; Osthoff, H.D.; Berlinguette, C.P. Electronic modification of the [Ru(II)(tpy)(bpy)(OH(2))](2+) scaffold: Effects on catalytic water oxidation. *J. Am. Chem. Soc.* **2010**, *132*, 16094–16106. [CrossRef] [PubMed]
24. Zhan, S.Q.; Zhang, B.B.; Sun, L.C.; Ahlquist, M.S.G. Hydrophobic/Hydrophilic Directionality Affects the Mechanism of Ru-Catalyzed Water Oxidation Reaction. *Acs Catal.* **2020**, *10*, 13364–13370. [CrossRef]
25. Yi, J.J.; Zhan, S.Q.; Chen, L.; Tian, Q.; Wang, N.; Li, J.; Xu, W.H.; Zhang, B.B.; Ahlquist, M.S.G. Electrostatic Interactions Accelerating Water Oxidation Catalysis via Intercatalyst O-O Coupling. *J. Am. Chem. Soc.* **2021**, *143*, 2484–2490. [CrossRef]
26. Dang, L.L.; Feng, H.J.; Lin, Y.J.; Jin, G.X. Self-Assembly of Molecular Figure-Eight Knots Induced by Quadruple Stacking Interactions. *J. Am. Chem. Soc.* **2020**, *142*, 18946–18954. [CrossRef] [PubMed]
27. Guo, X.; Wang, N.; Li, X.; Zhang, Z.; Zhao, J.; Ren, W.; Ding, S.; Xu, G.; Li, J.; Apfel, U.P.; et al. Homolytic versus Heterolytic Hydrogen Evolution Reaction Steered by a Steric Effect. *Angew. Chem. Int. Ed. Engl.* **2020**, *59*, 8941–8946. [CrossRef]
28. Liu, T.Q.; Zhan, S.Q.; Shen, N.N.; Wang, L.Q.; Szabo, Z.; Yang, H.; Ahlquist, M.S.G.; Sun, L.C. Bioinspired Active Site with a Coordination-Adaptive Organosulfonate Ligand for Catalytic Water Oxidation at Neutral pH. *J. Am. Chem. Soc.* **2023**, *145*, 11818–11828. [CrossRef]
29. Liu, T.Q.; Li, G.; Shen, N.N.; Wang, L.Q.; Timmer, B.J.J.; Zhou, S.Y.; Zhang, B.B.; Kravchenko, A.; Xu, B.; Ahlquist, M.S.G.; et al. Isolation and Identification of Pseudo Seven-Coordinate Ru(III) Intermediate Completing the Catalytic Cycle of Ru-bda Type of Water Oxidation Catalysts. *Ccs Chem.* **2022**, *4*, 2481–2490. [CrossRef]
30. Barnett, S.M.; Goldberg, K.I.; Mayer, J.M. A soluble copper-bipyridine water-oxidation electrocatalyst. *Nat. Chem.* **2012**, *4*, 498–502. [CrossRef]
31. Su, X.J.; Gao, M.; Jiao, L.; Liao, R.Z.; Siegbahn, P.E.; Cheng, J.P.; Zhang, M.T. Electrocatalytic water oxidation by a dinuclear copper complex in a neutral aqueous solution. *Angew. Chem. Int. Ed. Engl.* **2015**, *54*, 4909–4914. [CrossRef] [PubMed]
32. Hu, Q.Q.; Su, X.J.; Zhang, M.T. Electrocatalytic Water Oxidation by an Unsymmetrical Di-Copper Complex. *Inorg. Chem.* **2018**, *57*, 10481–10484. [CrossRef] [PubMed]

33. Su, X.J.; Zheng, C.; Hu, Q.Q.; Du, H.Y.; Liao, R.Z.; Zhang, M.T. Bimetallic cooperative effect on O-O bond formation: Copper polypyridyl complexes as water oxidation catalyst. *Dalton Trans.* **2018**, *47*, 8670–8675. [CrossRef]
34. Chen, Q.F.; Cheng, Z.Y.; Liao, R.Z.; Zhang, M.T. Bioinspired Trinuclear Copper Catalyst for Water Oxidation with a Turnover Frequency up to 20000 s(-1). *J. Am. Chem. Soc.* **2021**, *143*, 19761–19768. [CrossRef]
35. Fisher, K.J.; Materna, K.L.; Mercado, B.Q.; Crabtree, R.H.; Brudvig, G.W. Electrocatalytic Water Oxidation by a Copper(II) Complex of an Oxidation-Resistant Ligand. *Acs Catal.* **2017**, *7*, 3384–3387. [CrossRef]
36. Li, T.T.; Zheng, Y.Q. Electrocatalytic water oxidation using a chair-like tetranuclear copper(II) complex in a neutral aqueous solution. *Dalton T* **2016**, *45*, 12685–12690. [CrossRef]
37. Zhang, T.; Wang, C.; Liu, S.B.; Wang, J.L.; Lin, W.B. A Biomimetic Copper Water Oxidation Catalyst with Low Overpotential. *J. Am. Chem. Soc.* **2014**, *136*, 273–281. [CrossRef]
38. Ruan, G.; Fridman, N.; Maayan, G. Borate Buffer as a Key Player in Cu-Based Homogeneous Electrocatalytic Water Oxidation. *Chem-Eur. J.* **2022**, *28*, e202202407. [CrossRef]
39. Lin, J.Q.; Wang, N.N.; Chen, X.; Yang, X.L.; Hong, L.; Ruan, Z.J.; Ye, H.; Chen, Y.M.; Liang, X.M. Electrocatalytic water oxidation by copper(II) complexes with a pentadentate amine-pyridine ligand. *Sustain. Energ. Fuels* **2022**, *6*, 1312–1318. [CrossRef]
40. Jian, J.X.; Liao, J.X.; Zhou, M.H.; Yao, M.M.; Chen, Y.J.; Liang, X.W.; Liu, C.P.; Tong, Q.X. Enhanced Photoelectrochemical Water Splitting of Black Silicon Photoanode with pH-Dependent Copper-Bipyridine Catalysts. *Chem-Eur. J.* **2022**, *28*, e202201520. [CrossRef]
41. Mao, Q.Y.; Pang, Y.J.; Li, X.C.; Chen, G.J.; Tan, H.W. Theoretical Study of the Mechanisms of Two Copper Water Oxidation Electrocatalysts with Bipyridine Ligands. *Acs Catal.* **2019**, *9*, 8798–8809. [CrossRef]
42. Akbari, M.S.A.; Nandy, S.; Chae, K.H.; Bikas, R.; Kozakiewicz-Piekarz, A.; Najafpour, M.M. Water Oxidation by a Copper(II) Complex with 6,6?-Dihydroxy-2,2?-Bipyridine Ligand: Challenges and an Alternative Mechanism. *Langmuir* **2023**, *39*, 5542–5553. [CrossRef]
43. Gerlach, D.L.; Bhagan, S.; Cruce, A.A.; Burks, D.B.; Nieto, I.; Truong, H.T.; Kelley, S.P.; Herbst-Gervasoni, C.J.; Jernigan, K.L.; Bowman, M.K.; et al. Studies of the Pathways Open to Copper Water Oxidation Catalysts Containing Proximal Hydroxy Groups During Basic Electrocatalysis. *Inorg. Chem.* **2014**, *53*, 12689–12698. [CrossRef] [PubMed]
44. Koepke, S.J.; Light, K.M.; VanNatta, P.E.; Wiley, K.M.; Kieber-Emmons, M.T. Electrocatalytic Water Oxidation by a Homogeneous Copper Catalyst Disfavors Single-Site Mechanisms. *J. Am. Chem. Soc.* **2017**, *139*, 8586–8600. [CrossRef] [PubMed]
45. Shen, J.Y.; Wang, M.; Zhang, P.L.; Jiang, J.; Sun, L.C. Electrocatalytic water oxidation by copper(II) complexes containing a tetra- or pentadentate amine-pyridine ligand. *Chem. Commun.* **2017**, *53*, 4374–4377. [CrossRef]
46. Shen, J.Y.; Wang, M.; Gao, J.S.; Han, H.X.; Liu, H.; Sun, L.C. Improvement of Electrochemical Water Oxidation by Fine-Tuning the Structure of Tetradentate N-4 Ligands of Molecular Copper Catalysts. *Chemsuschem* **2017**, *10*, 4581–4588. [CrossRef]
47. Lee, H.; Wu, X.J.; Sun, L.C. Copper-based homogeneous and heterogeneous catalysts for electrochemical water oxidation. *Nanoscale* **2020**, *12*, 4187–4218. [CrossRef]
48. Lukacs, D.; Szyrwiel, L.; Pap, J.S. Copper Containing Molecular Systems in Electrocatalytic Water Oxidation-Trends and Perspectives. *Catalysts* **2019**, *9*, 83. [CrossRef]
49. Zhang, M.T.; Chen, Z.; Kang, P.; Meyer, T.J. Electrocatalytic water oxidation with a copper(II) polypeptide complex. *J. Am. Chem. Soc.* **2013**, *135*, 2048–2051. [CrossRef] [PubMed]
50. Pap, J.S.; Szyrwiel, L.; Sranko, D.; Kerner, Z.; Setner, B.; Szewczuk, Z.; Malinka, W. Electrocatalytic water oxidation by Cu(II) complexes with branched peptides. *Chem. Commun.* **2015**, *51*, 6322–6324. [CrossRef] [PubMed]
51. Szyrwiel, L.; Lukacs, D.; Ishikawa, T.; Brasun, J.; Szczukowski, L.; Szewczuk, Z.; Setner, B.; Pap, J.S. Electrocatalytic water oxidation influenced by the ratio between Cu(2+)and a multiply branched peptide ligand. *Catal. Commun.* **2019**, *122*, 5–9. [CrossRef]
52. Lukacs, D.; Nemeth, M.; Szyrwiel, L.; Illes, L.; Pecz, B.; Shen, S.H.; Pap, J.S. Behavior of a Cu-Peptide complex under water oxidation conditions—Molecular electrocatalyst or precursor to nanostructured CuO films? *Sol. Energ. Mat. Sol. C* **2019**, *201*, 110079. [CrossRef]
53. dos Santos, L.; Climent, V.; Blanford, C.F.; Armstrong, F.A. Mechanistic studies of the 'blue' Cu enzyme, bilirubin oxidase, as a highly efficient electrocatalyst for the oxygen reduction reaction. *Phys. Chem. Chem. Phys.* **2010**, *12*, 13962–13974. [CrossRef]
54. Goldfeder, M.; Kanteev, M.; Isaschar-Ovdat, S.; Adir, N.; Fishman, A. Determination of tyrosinase substrate-binding modes reveals mechanistic differences between type-3 copper proteins. *Nat. Commun.* **2014**, *5*, 4505. [CrossRef]
55. Fujieda, N.; Umakoshi, K.; Ochi, Y.; Nishikawa, Y.; Yanagisawa, S.; Kubo, M.; Kurisu, G.; Itoh, S. Copper-Oxygen Dynamics in the Tyrosinase Mechanism. *Angew. Chem. Int. Ed.* **2020**, *59*, 13385–13390. [CrossRef]
56. Kim, M.K.; Martell, A.E. Copper(2) Complexes of Triglycine and Tetraglycine. *J. Am. Chem. Soc.* **1966**, *88*, 914–918. [CrossRef]
57. Sanna, D.; Micera, G.; Kallay, C.; Rigo, V.; Sovago, I. Copper(II) complexes of N-terminal protected tri- and tetrapeptides containing histidine residues. *Dalton Trans.* **2004**, 2702–2707. [CrossRef] [PubMed]
58. Szyrwiel, L.; Szczukowski, L.; Pap, J.S.; Setner, B.; Szewczuk, Z.; Malinka, W. The Cu^{2+} Binding Properties of Branched Peptides Based on L-2,3-Diaminopropionic Acid. *Inorg. Chem.* **2014**, *53*, 7951–7959. [CrossRef]
59. Simon, R.J.; Kania, R.S.; Zuckermann, R.N.; Huebner, V.D.; Jewell, D.A.; Banville, S.; Ng, S.; Wang, L.; Rosenberg, S.; Marlowe, C.K.; et al. Peptoids: A modular approach to drug discovery. *Proc. Natl. Acad. Sci. USA* **1992**, *89*, 9367–9371. [CrossRef] [PubMed]

60. Zuckermann, R.N.; Kerr, J.M.; Kent, S.B.H.; Moos, W.H. Efficient Method for the Preparation of Peptoids [Oligo(N-Substituted Glycines)] by Submonomer Solid-Phase Synthesis. *J. Am. Chem. Soc.* **1992**, *114*, 10646–10647. [CrossRef]
61. Baskin, M.; Maayan, G. Water-Soluble Chiral Metallopeptoids. *Biopolymers* **2015**, *104*, 577–584. [CrossRef]
62. Baskin, M.; Maayan, G. A rationally designed metal-binding helical peptoid for selective recognition processes. *Chem. Sci.* **2016**, *7*, 2809–2820. [CrossRef] [PubMed]
63. Baskin, M.; Panz, L.; Maayan, G. Versatile ruthenium complexes based on 2,2′-bipyridine modified peptoids. *Chem. Commun.* **2016**, *52*, 10350–10353. [CrossRef]
64. Tigger-Zaborov, H.; Maayan, G. Nanoparticles assemblies on demand: Controlled aggregation of Ag(0) mediated by modified peptoid sequences. *J. Colloid. Interf. Sci.* **2017**, *508*, 56–64. [CrossRef]
65. Baskin, M.; Maayan, G. Chiral Cu(ii), Co(ii) and Ni(ii) complexes based on 2,2′-bipyridine modified peptoids. *Dalton Trans.* **2018**, *47*, 10767–10774. [CrossRef] [PubMed]
66. Baskin, M.; Zhu, H.; Qu, Z.W.; Chill, J.H.; Grimme, S.; Maayan, G. Folding of unstructured peptoids and formation of hetero-bimetallic peptoid complexes upon side-chain-to-metal coordination. *Chem. Sci.* **2019**, *10*, 620–632. [CrossRef] [PubMed]
67. D'Amato, A.; Ghosh, P.; Costabile, C.; Della Sala, G.; Izzo, I.; Maayan, G.; De Riccardis, F. Peptoid-based siderophore mimics as dinuclear Fe3+ chelators. *Dalton Trans.* **2020**, *49*, 6020–6029. [CrossRef]
68. Ghosh, P.; Maayan, G. A Water-Soluble Peptoid that Can Extract Cu2+ from Metallothionein via Selective Recognition. *Chem-Eur. J.* **2021**, *27*, 1383–1389. [CrossRef]
69. Behar, A.E.; Sabater, L.; Baskin, M.; Hureau, C.; Maayan, G. A Water-Soluble Peptoid Chelator that Can Remove Cu^{2+} from Amyloid-beta Peptides and Stop the Formation of Reactive Oxygen Species Associated with Alzheimer's Disease. *Angew. Chem. Int. Ed.* **2021**, *60*, 24588–24597. [CrossRef]
70. Jiang, L.H.; Hu, C.T.; De Riccardis, F.; Kirshenbaum, K. Elaborate Supramolecular Architectures Formed by Co-Assembly of Metal Species and Peptoid Macrocycles. *Cryst. Growth Des.* **2021**, *21*, 3889–3901. [CrossRef]
71. D'Amato, A.; Schettini, R.; Pierri, G.; Izzo, I.; Grisi, F.; Tedesco, C.; De Riccardis, F.; Costabile, C. Synthesis and characterization of new Na+ complexes of N-benzyl cyclic peptoids and their role in the ring opening polymerization of l-lactide. *New J. Chem.* **2021**, *45*, 5410–5420. [CrossRef]
72. Maayan, G.; Ward, M.D.; Kirshenbaum, K. Folded biomimetic oligomers for enantioselective catalysis. *Proc. Natl. Acad. Sci. USA* **2009**, *106*, 13679–13684. [CrossRef]
73. Prathap, K.J.; Maayan, G. Metallopeptoids as efficient biomimetic catalysts. *Chem. Commun.* **2015**, *51*, 11096–11099. [CrossRef] [PubMed]
74. Ghosh, T.; Ghosh, P.; Maayan, G. A Copper-Peptoid as a Highly Stable, Efficient, and Reusable Homogeneous Water Oxidation Electrocatalyst. *Acs Catal.* **2018**, *8*, 10631–10640. [CrossRef]
75. Darapaneni, C.M.; Ghosh, P.; Ghosh, T.; Maayan, G. Unique beta-Turn Peptoid Structures and Their Application as Asymmetric Catalysts. *Chem-Eur. J.* **2020**, *26*, 9573–9579. [CrossRef]
76. Ruan, G.; Engelberg, L.; Ghosh, P.; Maayan, G. A unique Co(III)-peptoid as a fast electrocatalyst for homogeneous water oxidation with low overpotential. *Chem. Commun.* **2021**, *57*, 939–942. [CrossRef]
77. Ruan, G.; Ghosh, P.; Fridman, N.; Maayan, G. A Di-Copper-Peptoid in a Noninnocent Borate Buffer as a Fast Electrocatalyst for Homogeneous Water Oxidation with Low Overpotential. *J. Am. Chem. Soc.* **2021**, *143*, 10614–10623. [CrossRef] [PubMed]
78. Culf, A.S.; Ouellette, R.J. Solid-Phase Synthesis of N-Substituted Glycine Oligomers (alpha-Peptoids) and Derivatives. *Molecules* **2010**, *15*, 5282–5335. [CrossRef]
79. Zborovsky, L.; Smolyakova, A.; Baskin, M.; Maayan, G. A Pure Polyproline Type I-like Peptoid Helix by Metal Coordination. *Chem-Eur. J.* **2018**, *24*, 1159–1167. [CrossRef]
80. Ghosh, P.; Torner, J.; Arora, P.S.; Maayan, G. Dual Control of Peptide Conformation with Light and Metal Coordination. *Chem-Eur. J.* **2021**, *27*, 8956–8959. [CrossRef]
81. Ghosh, T.; Fridman, N.; Kosa, M.; Maayan, G. Self-Assembled Cyclic Structures from Copper(II) Peptoids. *Angew. Chem. Int. Ed.* **2018**, *57*, 7703–7708. [CrossRef]
82. Ghosh, P.; Ruan, G.; Fridman, N.; Maayan, G. Amide bond hydrolysis of peptoids. *Chem. Commun.* **2022**, *58*, 9922–9925. [CrossRef] [PubMed]
83. Sun, J.Y.; Xu, H.Z. Synthesis, Structures and Properties of Cu(II) and Mn(II) Complexes with 1,10-Phenanthroline-2-carboxylic acid and 2,2′-Bipyridine Ligands. *Molecules* **2010**, *15*, 8349–8359. [CrossRef] [PubMed]
84. Constable, E.C.; Housecroft, C.E. Packing Motifs in [M(bpy)(2)X-2] Coordination Compounds (bpy=2,2′-bipyridine; X = F, Cl, Br, I). *Crystals* **2023**, *13*, 505. [CrossRef]
85. Mishra, B.K.; Sathyamurthy, N. pi-pi interaction in pyridine. *J. Phys. Chem. A* **2005**, *109*, 6–8. [CrossRef] [PubMed]
86. Hohenstein, E.G.; Sherrill, C.D. Effects of Heteroatoms on Aromatic pi-pi Interactions: Benzene-Pyridine and Pyridine Dimer. *J. Phys. Chem. A* **2009**, *113*, 878–886. [CrossRef]
87. Yu, F.S.; Li, F.; Hu, J.X.; Bai, L.C.; Zhu, Y.; Sun, L.C. Electrocatalytic water oxidation by a macrocyclic Cu(II) complex in neutral phosphate buffer. *Chem. Commun.* **2016**, *52*, 10377–10380. [CrossRef]
88. Xiang, R.J.; Wang, H.Y.; Xin, Z.J.; Li, C.B.; Lu, Y.X.; Gao, X.W.; Sun, H.M.; Cao, R. A Water-Soluble Copper-Polypyridine Complex as a Homogeneous Catalyst for both Photo-Induced and Electrocatalytic O-2 Evolution. *Chem-Eur. J.* **2016**, *22*, 1602–1607. [CrossRef]

89. Kafentzi, M.C.; Papadakis, R.; Gennarini, F.; Kochem, A.; Iranzo, O.; Le Mest, Y.; Le Poul, N.; Tron, T.; Faure, B.; Simaan, A.J.; et al. Electrochemical Water Oxidation and Stereoselective Oxygen Atom Transfer Mediated by a Copper Complex. *Chem-Eur. J.* **2018**, *24*, 5213–5224. [CrossRef]
90. Shahadat, H.M.; Younus, H.A.; Ahmad, N.; Zhang, S.G.; Zhuiykov, S.; Verpoort, F. Macrocyclic cyanocobalamin (vitamin B-12) as a homogeneous electrocatalyst for water oxidation under neutral conditions. *Chem. Commun.* **2020**, *56*, 1968–1971. [CrossRef]
91. Costentin, C.; Drouet, S.; Robert, M.; Savéant, J.-M. Correction to Turnover Numbers, Turnover Frequencies, and Overpotential in Molecular Catalysis of Electrochemical Reactions. Cyclic Voltammetry and Preparative-Scale Electrolysis. *J. Am. Chem. Soc.* **2012**, *134*, 19949–19950. [CrossRef]
92. Martin, D.J.; Mercado, B.Q.; Mayer, J.M. Combining scaling relationships overcomes rate versus overpotential trade-offs in O-2 molecular electrocatalysis. *Sci. Adv.* **2020**, *6*, eaaz3318. [CrossRef] [PubMed]
93. Artero, V.; Saveant, J.M. Toward the rational benchmarking of homogeneous H-2-evolving catalysts. *Energ. Env. Environ. Sci.* **2014**, *7*, 3808–3814. [CrossRef]
94. Garrido-Barros, P.; Funes-Ardoiz, I.; Drouet, S.; Benet-Buchholz, J.; Maseras, F.; Llobet, A. Redox Non-innocent Ligand Controls Water Oxidation Overpotential in a New Family of Mononuclear Cu-Based Efficient Catalysts. *J. Am. Chem. Soc.* **2015**, *137*, 6758–6761. [CrossRef] [PubMed]
95. Matheu, R.; Neudeck, S.; Meyer, F.; Sala, X.; Llobet, A. Foot of the Wave Analysis for Mechanistic Elucidation and Benchmarking Applications in Molecular Water Oxidation Catalysis. *Chemsuschem* **2016**, *9*, 3361–3369. [CrossRef]
96. Gentil, S.; Molloy, J.K.; Carriere, M.; Hobballah, A.; Dutta, A.; Cosnier, S.; Shaw, W.J.; Gellon, G.; Belle, C.; Artero, V.; et al. A Nanotube-Supported Dicopper Complex Enhances Pt-free Molecular H-2/Air Fuel Cells. *Joule* **2019**, *3*, 2020–2029. [CrossRef]
97. Zhang, X.F.; Li, Y.Y.; Jiang, J.; Zhang, R.; Liao, R.Z.; Wang, M. A Dinuclear Copper Complex Featuring a Flexible Linker as Water Oxidation Catalyst with an Activity Far Superior to Its Mononuclear Counterpart. *Inorg. Chem.* **2020**, *59*, 5424–5432. [CrossRef]
98. Geer, A.M.; Musgrave, C.; Webber, C.; Nielsen, R.J.; McKeown, B.A.; Liu, C.; Schleker, P.P.M.; Jakes, P.; Jia, X.F.; Dickie, D.A.; et al. Electrocatalytic Water Oxidation by a Trinuclear Copper(II) Complex. *Acs Catal.* **2021**, *11*, 7223–7240. [CrossRef]
99. Zhong, D.C.; Gong, Y.N.; Zhang, C.; Lu, T.B. Dinuclear metal synergistic catalysis for energy conversion. *Chem. Soc. Rev.* **2023**, *52*, 3170–3214. [CrossRef]
100. Kaeffer, N.; Morozan, A.; Fize, J.; Martinez, E.; Guetaz, L.; Artero, V. The Dark Side of Molecular Catalysis: Diimine-Dioxime Cobalt Complexes Are Not the Actual Hydrogen Evolution Electrocatalyst in Acidic Aqueous Solutions. *Acs Catal.* **2016**, *6*, 3727–3737. [CrossRef]
101. Wickramasinghe, L.D.; Zhou, R.W.; Zong, R.F.; Vo, P.; Gagnon, K.J.; Thummel, R.P. Iron Complexes of Square Planar Tetradentate Polypyridyl-Type Ligands as Catalysts for Water Oxidation. *J. Am. Chem. Soc.* **2015**, *137*, 13260–13263. [CrossRef] [PubMed]
102. Chen, Q.F.; Xiao, Y.; Liao, R.-Z.; Zhang, M.T. Trinuclear Nickel Catalyst for Water Oxidation: Intramolecular Proton-Coupled Electron Transfer Triggered Trimetallic Cooperative O–O Bond Formation. *CCS Chem.* **2023**, *5*, 245–256. [CrossRef]
103. Cao, R.; Saracini, C.; Ginsbach, J.W.; Kieber-Emmons, M.T.; Siegler, M.A.; Solomon, E.I.; Fukuzumi, S.; Karlin, K.D. Peroxo and Superoxo Moieties Bound to Copper Ion: Electron-Transfer Equilibrium with a Small Reorganization Energy. *J. Am. Chem. Soc.* **2016**, *138*, 7055–7066. [CrossRef]